A Laser-Shock-Enabled Hybrid Additive Manufacturing Strategy with Molten Pool Modulation of Fe-based Alloy

Jian Liu [a#], Shusen Zhao [b#], Xiaohan Zhang [a], Xuechun Lin [b*], Yaowu Hu [a*]

[a] The Institute of Technological Sciences, Wuhan University, Wuhan, 430072, China
[b] The Institute of Semiconductors, Chinese Academy of Sciences, Beijing, 100083, China
[#] Jian Liu and Shusen Zhao contributed equally to this work.
*Corresponding author: Yaowu Hu
E-mail: yaowuhu@whu.edu.cn
*Corresponding author: Xuechun Lin
E-mail: xclin@semi.ac.cn

Abstract

A novel hybrid laser additive manufacturing (LAM) process based on laser shock modulation of molten pool (LSMMP) is proposed in this work. By using a combination of experiment and simulation, the residual stress, heat transfer, and mass transfer behaviors are comprehensively studied. Also, microstructure evolution behavior is analyzed. The relationship between the convection behavior, the evolution of microstructure and the enhancement of residual stress induced by LSMMP is established. Compared with the traditional post-treatment process, the LSMMP assisted LAM process exhibits higher efficiency in residual stress control with the same pulsed laser energy input. The hidden mechanism in microstructure evolution and residual stress enhancement is expected to be possible related to intensified molten pool convection, uniform solute distribution and improved cooling rate induced by LSMMP. The hybrid LAM process strategy based on LSMMP provides a new approach for the application of short pulse laser in hybrid manufacturing.

Keywords: Additive manufacturing; Laser shock; Molten pool; Residual stress; Microstructure

1. Introduction

Compared with the subtractive manufacturing process, laser additive manufacturing (LAM) process, as a promising process that collect the wisdom of mechanics, materials, machinery, etc., presents inherent advantages in direct forming and remanufacturing fields [1–3]. Typical LAM process relied on the principle of layer by layer construction brings convenience to the direct forming of complex structural components, whereas it also has unavoidable disadvantages, such as geometry accuracy [4,5], metallurgical defects [6–8], and residual thermal stress [9,10]. The forming accuracy and surface roughness of LAM determine the manufacturing efficiency and forming quality of complex parts or dies. Metallurgical defects are generally the leading factor to induce the failure of parts, and the existence of residual stress significantly affects the fatigue properties of materials.

Generally, the residual stress determined by the layer-by-layer construction strategy and complex thermal history is inevitable in LAM process [11,12]. It has been revealed that the residual stress in LAM parts consists of two distinct zones, which are a compressive stress zone located in the middle area, and a tensile stress zone in the outer area [13], respectively. The residual stress distribution characteristics are related to the parts geometric, the thermophysical properties of the raw materials and the deposition path, since they directly affect the solidification behaviors of molten pool. Further, the parts geometry and the deposition path affect the residual stress by changing the heat transmission and diffusion processes, and thermophysical properties primarily influence the phase structure, microstructure and composition distribution, which are sensitive to the heat and mass transfer behaviors of molten pool. For example, the study on AISI H13 tool steel layers demonstrates that the compressive stresses is severely magnified by the martensite phase, which can be alleviated by proper heat treatment [14].

In response to the above-mentioned residual stress problem in LAM processes, a variety of post-treatment processes, including heat treatment [15], shot peening [16], ultrasonic surface mechanical grinding [17], ultrasonic impact [18], ultrasonic surface mechanical rolling [19], friction stir [20] and laser shock strengthening peening (LSP) [21–24], have been developed. In particular, ultra-high pressure plasma generated by short pulse laser is transmitted to the sample through shock wave in LSP process, resulting in ultra-high-strain-rate plastic deformation of

metals [25]. The implementation of LSP on metals proves that this process can induce the compressive stress as well as grain refinement, laying a foundation for the improvement of mechanical properties [26–28]. LSP, as an effective post- treatment technology, has achieved remarkable effect in residual stress enhancement. However, post-treatment is not conducive to process continuity and manufacturing efficiency of AM. Therefore, synchronous hybrid AM technology, which is an effective method that can reduce metallurgical defects and enhance the microstructure and residual stress of materials without increasing the total manufacturing time, is desirable, such as laser metal deposition process assisted with warm ultrasonic impact (LMD+WUI) [29], and LAM+LSP [30]. One issue that should be noted is that the core mechanism of the existing residual stress control technologies, including WUI and LSP, is to utilize the plastic deformation of the solidified surface, which requires a considerable shock pressure that exceeds the elastic limit. The shock pressure of LSP greatly depends on the restriction effectiveness provided by confinement layer on the laser-induced plasma. Unfortunately, it is difficult to lay the confinement layer in the continuous LAM process. Even though the above work can be achieved by moving the deposition layer from the AM platform to the LSP platform after each layer is deposited, but it is difficult to realize real-time residual stress control, and it will still extend the total processing time [31]. Therefore, aiming at the deficiency of poor synchronicity and low efficiency in the existing hybrid LAM process, we report a hybrid manufacturing strategy that combines LAM and laser shock modulation of molten pool (LSMMP) for the first time. Although short pulse laser is a commonly applied energy field in material properties enhancement, to our knowledge, there had not been any research on synchronous hybrid LAM process based on LSMMP. This method attempts to enhance the structure and residual stress of the cladding layer by LSMMP, and moves the pulsed laser irradiation area from the solid surface to the fluid molten pool, which can greatly reduce the shock pressure input requirements and solve the problem of confinement layer laying. In this paper, the molten pool morphology and microstructure of the cladding layers manufactured by LAM+LSMMP are studied by experimental observation and numerical simulation, and the distribution characteristics of residual stress are also considered. The relationship between the change of the convection behavior, the evolution of microstructure and the enhancement of residual stress induced by LSMMP is established. Also, the hidden mechanism of LSMMP to achieve the residual stress control and microstructure evolution of the cladding layer is discussed.

2. Experimental

2.1 Process and experimental design

As shown in Fig.1(a), the traditional LSP step is performed on the solidified cladding layer during LAM+LSP hybrid manufacturing process. In this work, the LAM+LSMMP hybrid process (Fig. 1(b)) moves the pulsed laser irradiation area into the liquid molten pool. Specifically, the Fe-based cladding layers were fabricated by LAM+LSMMP platform, which consists of a 3kW continuous-wave (CW) fiber laser using for LAM, a 3J pulse duration laser for LSMMP, and a 6-axis ABB robot arm for scanning track path implementation. The axes of the continuous wave laser beam and the pulse laser beam are symmetrically, deviating from the vertical direction by +5° and -5°, respectively. The raw material was supplied in the form of preset, and the thickness of preset powder was 0.7 mm. To suppress the metal oxidation behavior in the laser additive process, high-purity Ar was selected as the shielding gas. The gas feed rate was empirically set to 3 L/min. The energy of the CW laser were set as 1500 W. And the processing parameters of pulsed laser were as follows: 2 J pulse laser, 5 Hz repetition frequency. The beam diameter of the continuous wave laser and the pulse laser spot was 3 mm and 1.3 mm, respectively. The scanning speed of the CW laser was set to 4 mm/s.

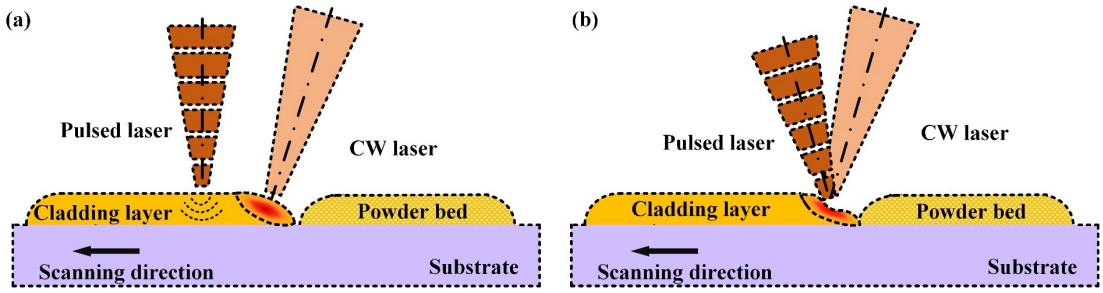

Fig. 1. Schematic diagram of LAM+LSMMP: (a) Traditional LAM+LSP process, (b) LAM+LSMMP in this study.

The LAM+LSMMP experiment was performed on a substrate of commercial AISI1045 steel. And acetone and alcohol were selected as detergents to remove impurities from the substrate surface. The Fe-based alloy powder (0.5 wt% C, 1.2 wt% Si, 1.6 wt% B, 0.8 wt% Mo, 13 wt% Cr, and Fe balance) was selected as the raw materials. The distance between the center of the two lasers was defined as the spot spacing, ranging from 0 mm to 4 mm. As a control sample, the original coating without laser shock processing was prepared as well. From Fig. 2, the pulsed laser radiates completely in the molten pool when the spot spacing is 0 mm, and with the broaden of spot spacing, the effective area of the pulsed laser acting on the molten pool becomes increasingly smaller. And the case where the spot spacing is greater than 2 mm is equivalent to the traditional LAM+LSP hybrid process shown in Fig. 1(a). Thereafter, the above samples were denoted as 0 J-0 mm, 2 J-0 mm, 2 J-1 mm, 2 J-2 mm, 2 J-3 mm. The real-time images of molten pool morphology during the LAM+LSMMP hybrid manufacturing process were collect by using high-speed camera. The specimens (10×10×10 mm^3) used for macroscopic morphology and microstructure characterization were cut from the cladding layers. The three-dimensional profile data of the coatings were recorded by white light interferometer. Microstructure observation was implemented by scanning electron microscope (SEM). The residual stress was measured by X-ray diffraction (XRD). Finite volume method (FVM) was utilized to simulate the convection behaviors and temperature distribution of the molten pool caused by LSMMP. Non-conforming mesh was used, and the unit size was also set to 0.4 mm. Residual stress was calculated by finite element method (FEM), among which the thermodynamic coupling model of LAM+LPS hybrid additive manufacturing process was established. PLANE13 quadrilateral four-node and SOLID5 hexahedron eight-node three-dimensional coupled field elements are selected. The overall mesh of the model was divided, and the mesh unit size was also set to 0.4 mm.

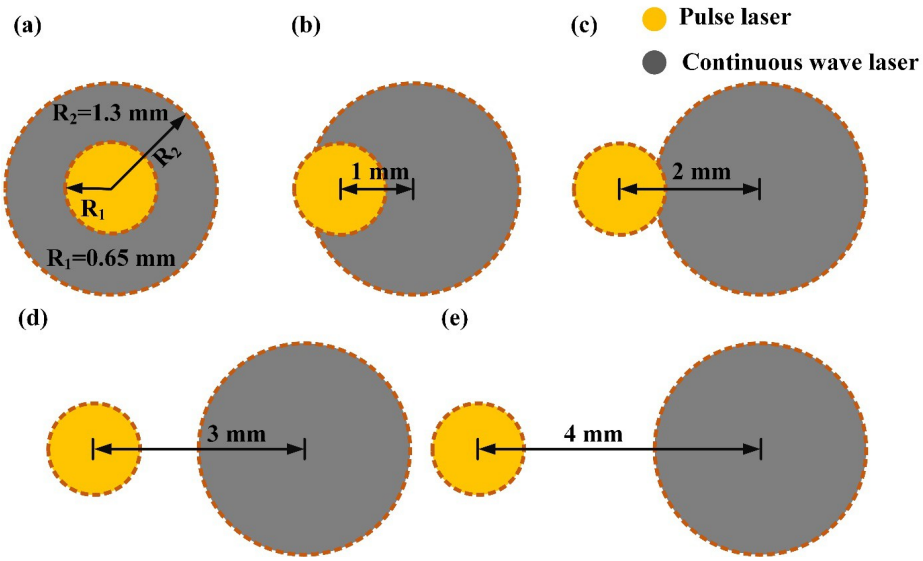

Fig. 2. Diagram of spot distribution of continuous and pulsed lasers.

3. Results and discussions

3.1 Residual stress

The residual stress curves of the cladding layers with various spot spacing is plotted in Fig.

3(a). The original coating without pulsed laser assistance presents a residual compressive stress of 332±18 MPa. It is obvious that the cladding layer with a spot spacing of 2 mm exhibits the largest residual compressive stress. It is considered that the cladding layer irradiated by the pulsed laser is in a mushy zone, which is more prone to plastic deformation than the completely solidified region. For the studied conditions and samples, the LSMMP-assisted LAM hybrid process (Spot spacing=0 mm, and 1mm) has a higher residual stress control efficiency than solid surface treatment (Spot spacing=3 mm, and 3mm). The contribution of LSMMP to the compressive stress in the upper zone of the cladding layers is significantly reduced, when the spot spacing is greater than 2 mm. This phenomenon is generated by the surface state variation of the region acted by the pulse laser. As the pulsed laser gradually deviates from the center of the molten pool, the physical state of the area of the pulsed laser irradiation evolves from a molten state to a semi-solidified state, and then completely changes to a solidified state. Such a sharp increase in surface strength in turn weakens the acting effect of the pulsed laser with limited energy. Furthermore, form Fig.3 (b) and (c), the compressive residual stress area located in the center zone is contractive, while the tensile stress in the substrate shows a decreasing trend. The above results demonstrate the effectiveness of the LSMMP strategy, and the hidden mechanism of LSMMP to achieve the residual stress control of the cladding layer will be discussed later.

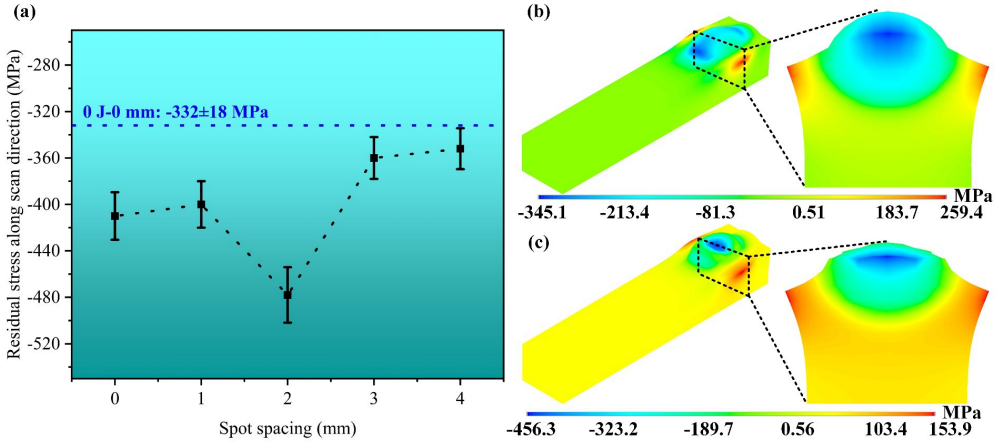

Fig. 3. Experimental and simulation results of the cladding layers: (a) Experimental results, (b) Simulation results of 0 J-0 mm, (c) Simulation results of 2 J-0 mm.

3.2 Macro-morphology

The 3D profiles of single-track cladding layers with different spot spacing are shown in Fig.4. It can be found that the most noticeable feature is that the introduction of pulsed laser energy fields during AM promotes the formation of perlage on the surface of the cladding layers under the condition of small spot spacing (≤2 mm). However, the surface morphologies of the cladding layers fabricated at large spot spacing (>2mm) is semblable to that of the original coating 0 J-0 mm, since the pulse laser applied to the surface of metal, which is in the solidified or semi-solidified state, causes slight plastic deformation diminutively. The modulate effect of surface morphology is closely related to spot spacing, where the achievements of LSMMP on molten pool morphology weakens with the increase of spot spacing.

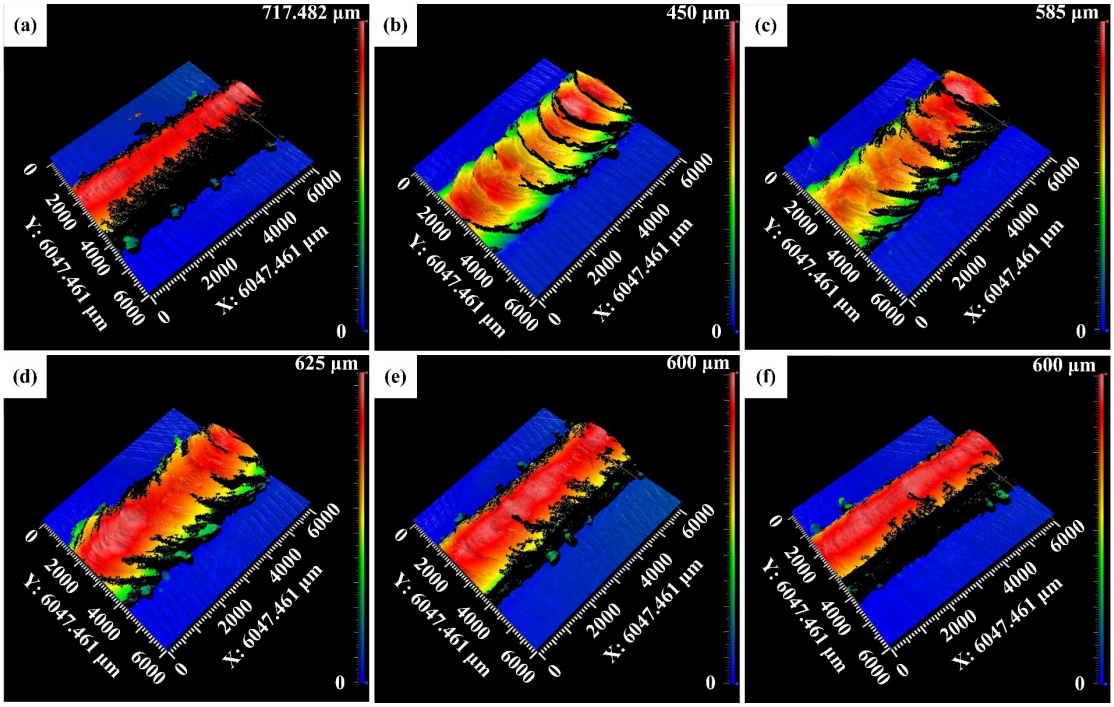

Fig. 4. 3D profiles of cladding layers with different spot spacing: (a) 0 J-0 mm, (b) 2 J -0 mm, (c) 2 J -1 mm, (d) 2 J -2 mm, (e) 2 J -3 mm, (f) 2 J -4 mm.

The 2D cross-section profiles (Fig.5) of the cladding layers with various spot distance reveal the effectiveness of LSMMP to width to height ratio of the molten pool during AM process. Since the molten pool bears the complete laser-induced shock wave pressure, Sample 2 J-0 mm shows the prominent improvement effect. Specifically, compared with the original sample 0 J-0 mm, the height of sample 2 J-0 mm decreased by about 43%, and the width increased by about 7%. In particular, the height of the 2 J-3 mm and 2 J-4 mm samples show only a slight decrease, which is consistent with the variation trend of residual stress.

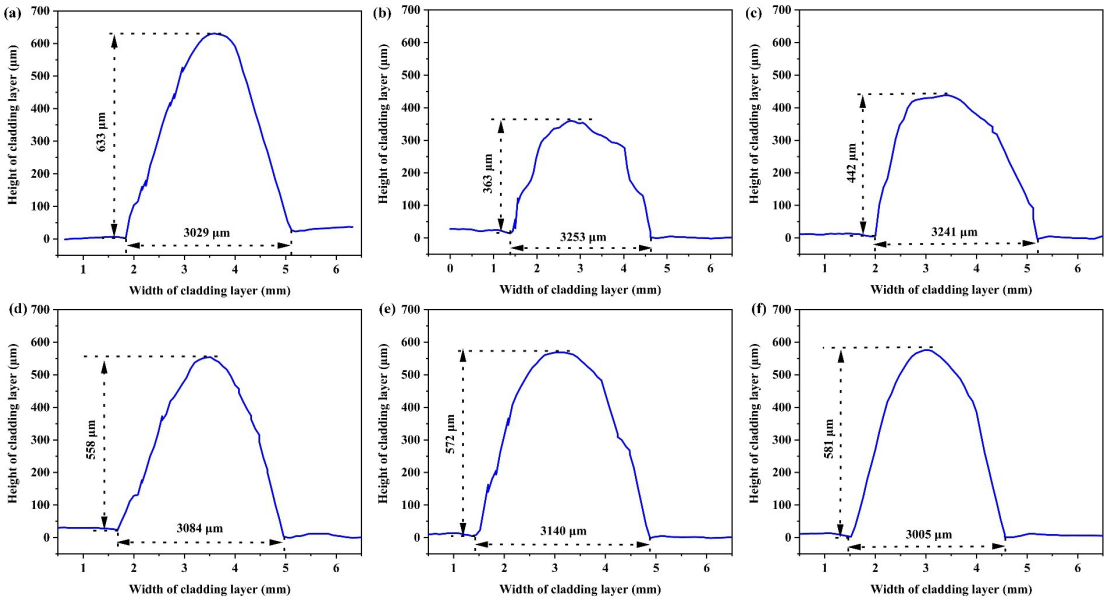

Fig. 5. 2D cross-section profiles of cladding layer: (a) 0 J-0 mm, (b) 2 J-0 mm, (c) 2 J-1 mm, (d) 2 J-2 mm, (e) 2 J-3 mm, (f) 2 J-4 mm.

3.3 Microstructure evolution

The cross-section SEM image in Fig.6(a) indicates that the cladding layer exhibits excellent forming quality. The typical metallurgical defects, including cracks and voids, are not observed in the dense coatings. From Fig. 6(b), It can be found that the Fe-based cladding layers presents typical dendritic structure. The enlarged SEM image in Fig.6(c) reveals that the interdendritic

region (IR) consists of eutectic phase with a continuous network-shape, and the dendritic region (DR) is constituted by residual austenite and lath martensite. This is consistent with the results of previous studies [32]. The IR phase is formed by eutectic reaction of austenite and boride, because B element tends to segregate and precipitate to austenite grain boundary, which can be proved by chemical composition distribution (DR: 38.35 at.% C, 0.39 at.% Si, 1.21 at.% Cr, 0.70 at.% Mo, 59.36 at.% Fe; IR: 34.41 at.% C, 0.18 at.% Si, 1.90 at.% Cr, 0.73 at.% Mn, 45.03 at.% Fe, 17.75 at.% B). Additionally, the eutectic borides in Fe-based alloys has a crystal structure of M_2B (M is Fe, Cr or Mn) [33].

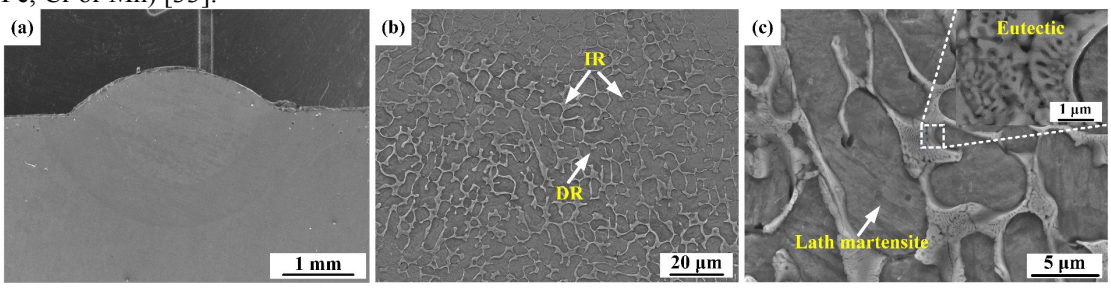

Fig. 6. SEM images of cladding layers: (a) cross-section SEM image, (b) microstructure image, (c) Enlarged SEM image.

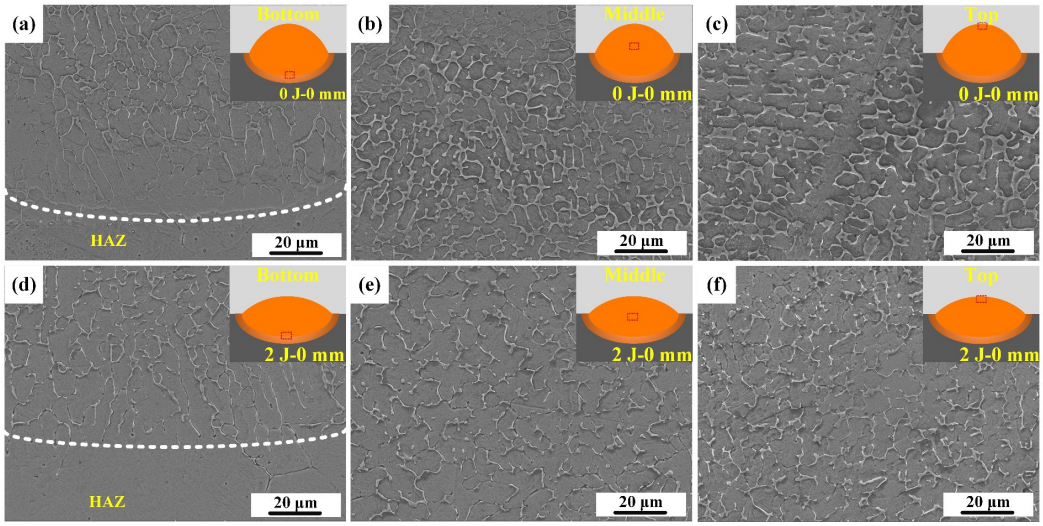

Fig. 7. Cross-section SEM images of the cladding layers along different depths direction: (a)-(c) 0 J-0 mm, (d)-(f) 2 J-0 mm.

As shown in Fig. 7, microstructure at different depths along the cross-section of the cladding layers are observed comprehensively, to explore the influence of laser shock modulation of molten pool in LAM on the solidification process. The observation positions are roughly shown in the illustration of the corresponding SEM image. From Fig. 7(a) and (c), both samples exhibit columnar dendrites perpendicular to the bonding interface in the bottom area. There is no significant difference in the microstructure near the interface implying that the effect of the pulsed laser on the morphology modulation and solidification process of the bottom of the molten pool is almost negligible. However, the distribution characteristics of the dendrite morphology in the middle and top areas of samples 0 J-0 mm and 2 J-0 mm are significantly diverse. The adjacent eutectic phases in sample 0 J-0 mm appear parallel distribution, which is determined by the steady heat flow diffusion behavior. In contrast, the eutectic phase in the top and middle areas of 2 J-0 mm present a disordered distribution characteristic, meaning that the growth behavior of grains with preferred orientation is broken by external energy field of the pulsed laser. The stability of the front end of the solid-liquid interface in the solidification process is destroyed by the molten pool oscillation, which inhibits the directional growth behavior of dendrite. Additionally, it is worth noting that the influence of the external energy field on solidification behavior is also reflected in the distribution characteristics and phase volume fraction of the eutectic. By comparing Fig. 7(b)and (e), or (c) and (f), it can be perceived that the eutectic phase with continuous network-shape is transformed into a discontinuous and refined state. The calculation results of the volume fraction show that the fraction of the IR at the bottom, middle

and upper areas of sample 0 J-0 mm are 6.41%,17.03% and 16.55%, while those in sample 2 J-0 mm are 6.20%, 10.17%, 9.96%, respectively. It can be found that the influence of LSMMP process on the microstructure is mainly reflected in the middle and upper part of the cladding layer. It is believed that the change in heat transfer behavior caused by the forced oscillation of the molten pool is the critical factor that induces the above phenomenon. It was reported that a slow cooling rate is more conducive to the precipitation of borides [34]. Also, we speculates that the increase of volume fraction of martensite matrix is related to the increase of cooling rate caused by molten pool oscillation [35]. In this study, the LSMMP drives the oscillation of the molten pool, which promotes the thermal diffusion process in the middle and upper part of the molten pool and increases the solidification rate, thus inhibiting the eutectic reaction and accelerating the martensitic transformation.

3.4 Molten pool flow behavior

To explore the modulation effect of pulsed laser on molten pool, real-time images of molten pool evolution were collected. Fig. 8(a)-(c) record the advancing process of the molten pool of sample 0 J-0 mm. The liquid droplets formed by laser fusion gradually converge into the plump molten pool. Unlike the molten pool features of the initial cladding layer without LSMMP process, the pulsed laser-induced bright plasma can be found (Fig. 8(d)). Most significantly, pulsed laser can effectively drive the morphological transformation of molten pool from plump to flat shape (Fig. 8(e)) depending on the forced vibration of the molten pool actuated by the shock pressure. Besides, a slight fluctuation dominated by surface tension was observed in the 3 ms to 4 ms after the pulsed laser was applied (Fig. 8(f)). Thus, the formation of the perlage and sub-perlage presented in Fig. 4(b)-(d) can be explained by the forced fluctuation of molten pool driven by LSMMP and the slight vibration dominated by surface tension of molten pool, respectively.

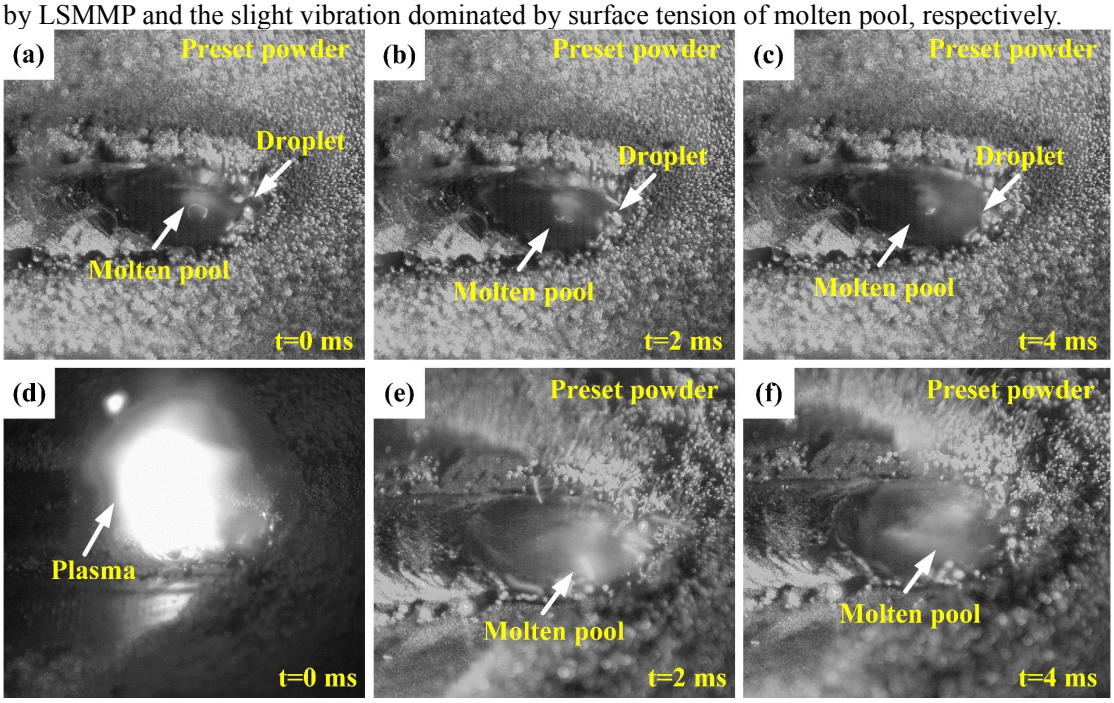

Fig. 8. Real-time images of molten pool evolution: (a)-(c) 0 J-0 mm, (d)-(f) 2 J-0 mm.

The hidden mechanism of LSMMP to achieve the residual stress control and microstructure evolution of the cladding layer is discussed from the perspective of the change of the convection state of the molten pool. Fig. 9(a) displays the molten pool without LSMMP (0 J-0 mm) assistance. The plump molten pool presents a pair of symmetrical convection rings, which travel down the vertical centerline to the solid-liquid interface. And then surging toward the upper surface of the cladding layer on both sides. A distinct morphology, where a pit appears in the pulsed laser irradiation area, can be observed in the molten pool assisted by LSMMP (Fig. 9(b)). Furtherly, there is a significant change in the molten pool convection behavior at the unloading stage of the pulsed laser-induced plasma shock wave, especially below-central area of the molten pool. It can be found from Fig. 9(c), that the middle and upper area of the flat molten pool forms a pair of symmetrical convection rings that is opposite to the flow direction of the 0 J-0 mm (Fig.

9(a)), while no apparent disturbance flow behavior is observed near the interface. Thus, it is expected that the microstructure evolution and residual stress enhancement by the LAM+LSMMP may be related to one or both of the following possible mechanisms: (i) The LSMMP process intensifies the flow behavior of molten pool, resulting in the increased solidification rate, suppressed borides precipitation, and accelerated martensitic transformation processes. (ii) The molten pool convection facilitated by LSMMP is beneficial to the diffusion and uniform distribution of solute, which reduces the possibility of precipitation at grain boundary. (iii) The accelerated martensite precipitation process leads to an increased residual compressive stress [14].

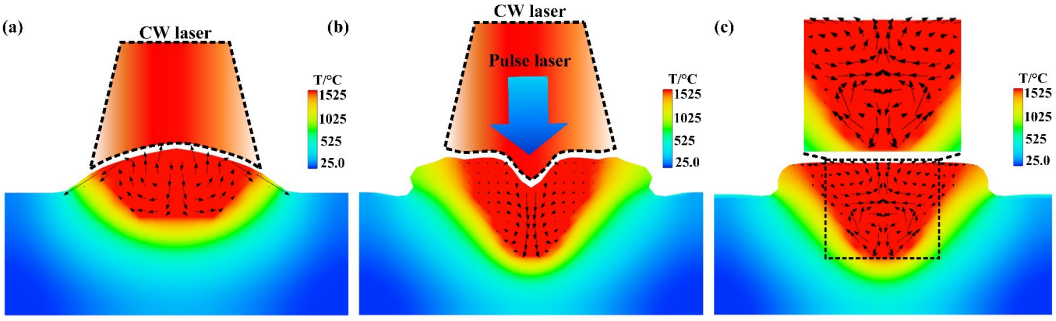

Fig. 9. Simulation results of molten pool convection: (a) Convection without LSMMP assistance, (b) Convection with LSMMP loading process, (c) Convection with LSMMP unloading process.

In summary, the LSMMP assisted LAM hybrid process transfers the pulsed laser irradiation area from the solid or semi-condensed solid metal surface to the liquid molten pool area, and obtains more efficient residual stress control effect under fixed low laser energy input conditions. Compared with the strategy of improving the shock pressure on the solid surface by increasing the pulse laser energy or laying a confinement layer in an inconvenient way, the LSMMP assisted LAM process proposed in this study may have lower production costs and total manufacturing time. This seemingly simple hybrid process is also expected to be applied to highly brittle and easy-to-crack additive materials caused by unfavorable precipitation phases at grain boundaries, thanks to the solute convection and uniform distribution promoted by LSMMP process.

4. Conclusions

In this content, we attempt to enhance the microstructure and residual stress of the materials through the disturbance of the molten pool, and propose a LAM and LSMMP hybrid manufacturing strategy. Different from the traditional LSP process, the pulsed laser irradiation area is moved from the solid surface to the liquid molten pool. For the conditions and samples studied, the LSMMP assisted LAM hybrid process exhibits higher efficiency in residual stress control than traditional LAM+LSP with the same pulsed laser energy input. Combined with the pool morphology observation and simulation results, it is analyzed that the hidden mechanism in microstructure evolution and residual stress enhancement is expected to be possible related to intensified molten pool convection, uniform solute distribution and improved cooling rate induced by LSMMP. The LSMMP process intensifies and changes the flow behavior of the molten pool, increases the solidification rate, inhibits the intergranular precipitation and accelerates the martensitic transformation. The proposed LAM and LSMMP hybrid manufacturing process could be implemented to control the fluid flow, heat and mass transfer during fusion joining and additive manufacturing, which is critical to geometric accuracies, composition distribution, precipitation phases, microstructures, stress states and mechanical properties.

Acknowledgements

This work was supported by the National Natural Science Foundation of China (Grant No. 51901162 and U2033211). The authors thank the support of the National Talent Program of China.

Reference

[1] D. Gu, X. Shi, R. Poprawe, D.L. Bourell, R. Setchi, J. Zhu, Material-structure-performance integrated laser-metal additive manufacturing, Science (80-.). 372 (2021) https://doi.org/10.1126/science.abg1487.

[2] D.L. Bourell, D.W. Rosen, M.C. Leu, The roadmap for additive manufacturing and its impact, 3D Print. Addit. Manuf. 1 (2014) 6–9. https://doi.org/10.1089/3dp.2013.0002.
[3] S.E. Brika, M. Letenneur, C.A. Dion, V. Brailovski, Influence of particle morphology and size distribution on the powder flowability and laser powder bed fusion manufacturability of Ti-6Al-4V alloy, Addit. Manuf. 31 (2020) 100929. https://doi.org/10.1016/j.addma.2019.100929.
[4] S. Hällgren, L. Pejryd, J. Ekengren, 3D Data Export for Additive Manufacturing-Improving Geometric Accuracy, Procedia CIRP. 50 (2016) 518–523. https://doi.org/10.1016/j.procir.2016.05.046.
[5] P. Minetola, M. Galati, A challenge for enhancing the dimensional accuracy of a low-cost 3D printer by means of self-replicated parts, Addit. Manuf. 22 (2018) 256–264. https://doi.org/10.1016/j.addma.2018.05.028.
[6] S. Cooke, K. Ahmadi, S. Willerth, R. Herring, Metal additive manufacturing: Technology, metallurgy and modelling, J. Manuf. Process. 57 (2020) 978–1003. https://doi.org/10.1016/j.jmapro.2020.07.025.
[7] A. Hilaire, E. Andrieu, X. Wu, High-temperature mechanical properties of alloy 718 produced by laser powder bed fusion with different processing parameters, Addit. Manuf. 26 (2019) 147–160. https://doi.org/10.1016/j.addma.2019.01.012.
[8] W.J. Sames, F.A. List, S. Pannala, R.R. Dehoff, S.S. Babu, The metallurgy and processing science of metal additive manufacturing, Int. Mater. Rev. 61 (2016) 315–360. https://doi.org/10.1080/09506608.2015.1116649.
[9] G. Sander, A.P. Babu, X. Gao, D. Jiang, N. Birbilis, On the effect of build orientation and residual stress on the corrosion of 316L stainless steel prepared by selective laser melting, Corros. Sci. 179 (2021) 109149. https://doi.org/10.1016/j.corsci.2020.109149.
[10] O. Fergani, F. Berto, T. Welo, S.Y. Liang, Analytical modelling of residual stress in additive manufacturing, Fatigue Fract. Eng. Mater. Struct. 40 (2017) 971–978. https://doi.org/10.1111/ffe.12560.
[11] D.D. Gu, W. Meiners, K. Wissenbach, R. Poprawe, Laser additive manufacturing of metallic components: Materials, processes and mechanisms, Int. Mater. Rev. 57 (2012) 133–164. https://doi.org/10.1179/1743280411Y.0000000014.
[12] W.E. Frazier, Metal additive manufacturing: A review, J. Mater. Eng. Perform. 23 (2014) 1917–1928. https://doi.org/10.1007/s11665-014-0958-z.
[13] P. Mercelis, J.P. Kruth, Residual stresses in selective laser sintering and selective laser melting, Rapid Prototyp. J. 12 (2006) 254–265. https://doi.org/10.1108/13552540610707013.
[14] N.S. Bailey, C. Katinas, Y.C. Shin, Laser direct deposition of AISI H13 tool steel powder with numerical modeling of solid phase transformation, hardness, and residual stresses, J. Mater. Process. Technol. 247 (2017) 223–233. https://doi.org/10.1016/j.jmatprotec.2017.04.020.
[15] C.R. Knowles, T.H. Becker, R.B. Tait, The effect of heat treatment on the residual stress levels within direct metal laser sintered ti-6al-4v as measured using the hole-drilling strain gauge method, Rapdasa. 23 (2012) 119–129.
[16] N.E. Uzan, S. Ramati, R. Shneck, N. Frage, O. Yeheskel, On the effect of shot-peening on fatigue resistance of AlSi10Mg specimens fabricated by additive manufacturing using selective laser melting (AM-SLM), Addit. Manuf. 21 (2018) 458–464. https://doi.org/10.1016/j.addma.2018.03.030.
[17] X. Yan, S. Yin, C. Chen, R. Jenkins, R. Lupoi, R. Bolot, W. Ma, M. Kuang, H. Liao, J. Lu, M. Liu, Fatigue strength improvement of selective laser melted Ti6Al4V using ultrasonic surface mechanical attrition, Mater. Res. Lett. 7 (2019) 327–333. https://doi.org/10.1080/21663831.2019.1609110.
[18] M. Zhang, C. Liu, X. Shi, X. Chen, C. Chen, J. Zuo, J. Lu, S. Ma, Residual stress, defects and grain morphology of ti-6al-4v alloy produced by ultrasonic impact treatment assisted selective laser melting, Appl. Sci. 6 (2016) 1–7. https://doi.org/10.3390/app6110304.
[19] Z. Wang, Z. Liu, C. Gao, K. Wong, S. Ye, Z. Xiao, Modified wear behavior of selective laser melted Ti6Al4V alloy by direct current assisted ultrasonic surface rolling process, Surf. Coatings Technol. 381 (2020) 125122. https://doi.org/10.1016/j.surfcoat.2019.125122.
[20] A.H. Maamoun, S.C. Veldhuis, M. Elbestawi, Friction stir processing of AlSi10Mg parts produced by selective laser melting, J. Mater. Process. Technol. 263 (2019) 308–320. https://doi.org/10.1016/j.jmatprotec.2018.08.030.
[21] N. Kalentics, E. Boillat, P. Peyre, S. Ćirić-Kostić, N. Bogojević, R.E. Logé, Tailoring residual stress profile of Selective Laser Melted parts by Laser Shock Peening, Addit. Manuf. 16 (2017) 90–97. https://doi.org/10.1016/j.addma.2017.05.008.
[22] D. Lin, M. Motlag, M. Saei, S. Jin, R.M. Rahimi, D. Bahr, G.J. Cheng, Shock engineering the

additive manufactured graphene-metal nanocomposite with high density nanotwins and dislocations for ultra-stable mechanical properties, Acta Mater. 150 (2018) 360–372. https://doi.org/10.1016/j.actamat.2018.03.013.
[23] Z. Tong, H. Liu, J. Jiao, W. Zhou, Y. Yang, X. Ren, Improving the strength and ductility of laser directed energy deposited CrMnFeCoNi high-entropy alloy by laser shock peening, Addit. Manuf. 35 (2020) 101417. https://doi.org/10.1016/j.addma.2020.101417.
[24] Z. Tong, H. Liu, J. Jiao, W. Zhou, Y. Yang, X. Ren, Microstructure, microhardness and residual stress of laser additive manufactured CoCrFeMnNi high-entropy alloy subjected to laser shock peening, J. Mater. Process. Technol. 285 (2020) 116806. https://doi.org/10.1016/j.jmatprotec.2020.116806.
[25] M. Dorman, M.B. Toparli, N. Smyth, A. Cini, M.E. Fitzpatrick, P.E. Irving, Effect of laser shock peening on residual stress and fatigue life of clad 2024 aluminium sheet containing scribe defects, Mater. Sci. Eng. A. 548 (2012) 142–151. https://doi.org/10.1016/j.msea.2012.04.002.
[26] K.Y. Luo, X. Jing, J. Sheng, G.F. Sun, Z. Yan, J.Z. Lu, Characterization and analyses on micro-hardness, residual stress and microstructure in laser cladding coating of 316L stainless steel subjected to massive LSP treatment, J. Alloys Compd. 673 (2016) 158–169. https://doi.org/10.1016/j.jallcom.2016.02.266.
[27] W. Guo, R. Sun, B. Song, Y. Zhu, F. Li, Z. Che, B. Li, C. Guo, L. Liu, P. Peng, Laser shock peening of laser additive manufactured Ti6Al4V titanium alloy, Surf. Coatings Technol. 349 (2018) 503–510. https://doi.org/10.1016/j.surfcoat.2018.06.020.
[28] S. Luo, W. He, K. Chen, X. Nie, L. Zhou, Y. Li, Regain the fatigue strength of laser additive manufactured Ti alloy via laser shock peening, J. Alloys Compd. 750 (2018) 626–635. https://doi.org/10.1016/j.jallcom.2018.04.029.
[29] H. Song, M. Li, M. Wang, B. Wu, Z. Liu, H. Ding, W. Liu, Preliminary experimental study of warm ultrasonic impact-assisted laser metal deposition, J. Manuf. Sci. Eng. Trans. ASME. 143 (2021) 1–5. https://doi.org/10.1115/1.4049645.
[30] J. Lu, H. Lu, X. Xu, J. Yao, J. Cai, K. Luo, High-performance integrated additive manufacturing with laser shock peening –induced microstructural evolution and improvement in mechanical properties of Ti6Al4V alloy components, Int. J. Mach. Tools Manuf. 148 (2020) 103475. https://doi.org/10.1016/j.ijmachtools.2019.103475.
[31] N. Kalentics, K. Huang, M. Ortega Varela de Seijas, A. Burn, V. Romano, R.E. Logé, Laser shock peening: A promising tool for tailoring metallic microstructures in selective laser melting, J. Mater. Process. Technol. 266 (2019) 612–618. https://doi.org/10.1016/j.jmatprotec.2018.11.024.
[32] W. Gao, S. Zhao, Y. Wang, Z. Zhang, C. Zhou, X. Lin, Refinement of Fe-based alloy doped Ti cladding layer, Surf. Coatings Technol. 270 (2015) 16–23. https://doi.org/10.1016/j.surfcoat.2015.03.024.
[33] Z. li LIU, X. CHEN, Y. xiang LI, K. hua HU, High Boron Iron-Based Alloy and Its Modification, J. Iron Steel Res. Int. 16 (2009) 37-42,54. https://doi.org/10.1016/S1006-706X(09)60041-8.
[34] I. Fedorova, F. Liu, F.B. Grumsen, Y. Cao, O. V. Mishin, J. Hald, Fine (Cr,Fe)2B borides on grain boundaries in a 10Cr–0.01B martensitic steel, Scr. Mater. 156 (2018) 124–128. https://doi.org/10.1016/j.scriptamat.2018.07.021.
[35] J.H. Liu, N. Binot, D. Delagnes, M. Jahazi, Influence of the cooling rate below Ms on the martensitic transformation in a low alloy medium-carbon steel, J. Mater. Res. Technol. 12 (2021) 234–242. https://doi.org/10.1016/j.jmrt.2021.02.075.